Research Article Vol. 29, No. 6 / 15 March 2021 / Optics Express 9217
Optics EXPRESS

Polarization holographic recording of vortex diffractive optical elements on azopolymer thin films and 3D analysis via phase-shifting digital holographic microscopy

VERONICA CAZAC,[1,2,*] ELENA ACHIMOVA,[1] VLADIMIR ABASHKIN,[1] ALEXANDR PRISACAR,[1] CONSTANTIN LOSHMANSCHII,[1] ALEXEI MESHALKIN,[1] AND KAREN EGIAZARIAN[2]

[1] *Laboratory of Materials for Photovoltaics and Photonics, Institute of Applied Physics, 5 Academiei str., MD-2028, Chisinau, Moldova*
[2] *Faculty of Information Technology and Communication Sciences, Tampere University, Korkeakoulunkatu 1, FI-33720, Finland*
[*] *veronica.cazac@tuni.fi*

Abstract: Direct fabrication of complex diffractive optical elements (DOEs) on photosensitive thin films is of critical importance for the development of advanced optical instruments. In this paper, we design and investigate DOEs capable of generating optical vortices. Analog and digital approaches for one-step polarization holographic recording of vortex DOEs on new carbazole-based azopolymer thin films are described. First configuration involves analog polarization holographic recording using a vortex phase retarder and has as a result the DOE producing a diffraction pattern with phase singularities aligned in a single line. Similar diffraction picture is achieved by the single-beam digital holographic recording setup with an integrated spatial light modulator. In the third system, the implemented double-beam digital polarization holographic recording setup yields simultaneously a spatial multiplexed vortex pattern. Diffraction efficiency evolution of these three types of DOEs are monitored and compared. The phase-shifting digital holographic microscope with an electrically controlled liquid crystal variable retarder is applied to investigate the phase and surface topography of the inscribed diffractive optical elements. The comparison between the digital and analog micro-patterning techniques contributes new evidence to limited data on the influence of the analog and digital generation of the spiral wavefront on the performance of vortex DOEs.

1. Introduction

The electromagnetic wave twisted around the propagation axis possessing a phase singularity, an orbital angular momentum (OAM) and a topological charge (TC) is called an optical vortex (OV). The phase singularity defines the zero intensity and indeterminate phase region of the optical field, while the OAM provides an additional degree of freedom for the structured light [1]. Design of optical elements which produce this type of light field is one of the hot frontiers in various branches of modern technology that use accurately shaped helical wavefronts to control diverse optical systems [2–4]. However, the generation, manipulation, and detection of OAM is still challenging. Among different optical components that produce light fields with doughnut intensity distribution [5–9], DOEs generate OAM states efficiently, compactly with a particular phase distribution and tolerance to input polarization [10].

Thirty years of research on phase singularities gave rise to several techniques for fabrication of DOEs as photolithography [11,12], focused ion beam writing [13], and holography [14]. Although most of these techniques provide good quality DOE, time-consuming procedures

#415639 https://doi.org/10.1364/OE.415639
Journal © 2021 Received 26 Nov 2020; revised 29 Jan 2021; accepted 20 Feb 2021; published 10 Mar 2021

Optics EXPRESS

involving numerous processing stages is the main problem, especially when encumbering etching procedures are required. In contrast with the regular holography, polarization holographic recording (PHR) triggers the mass transport mechanisms that leads to deeper surface relief formation exclusive of extra post-processing. Furthermore, polarization holography is operating with different polarization states of the recording beams, and makes it possible to reveal the phase features of the vortex DOEs [15]. It implies recording of the interference between a reference beam and a modified spiral-shaped beam with orthogonal polarizations of both beams. The design of the interferometric setup allows the operation of a spatial light modulator (SLM), useful for digital control of the TC of the generated phase singularities as well as the formation of sophisticated vortex-shaped structures.

The quality of the complex diffractive structures is determined not only by the recording techniques but also by the properties of light-responsive materials. In fact, for performing successful PHR it is important to select an appropriate material that is both photo- and polarization-sensitive. Thanks to induced anisotropy, azopolymers thin layers possess both properties, and are suitable for micro- and nano-patterning via PHR [16,17]. Moreover, remarkable optical and structural proprieties of amorphous azopolymer thin films allow one-step formation of complex surface relief structures capable of producing spatial multiplexed vortex patterns.

Nevertheless, another issue in development of qualitative vortex DOEs is the microscopic non-contact, in-depth analysis of the phase and surface changes. The digital holographic microscope (DHM) performs non-invasive monitoring of transparent samples' phase and amplitude [18,19]. Owing to the quantitative phase data, obtained by DHM, it allows a detailed visualization of DOE, otherwise invisible via current commercial light microscopes. This is a full-field imaging technique, and is essential for understanding the evolution of complex three-dimensional (3D) structures created inside transparent materials, where the scanning microscopes such as atomic force microscope or scanning electron microscope cannot be applied.

The contribution of this paper concerns: a) the design and characterization of three types of DOEs capable of generating single and multi-channel vortex beams via one-step relief formation on carbazole-based azopolymer thin films by analog and digital PHR (without chemical etching), b) the upgrade of the phase-shifting digital holographic microscope (PS-DHM) with a liquid crystal variable retarder for producing all-optical phase-shifts, and c) the detailed investigation of the phase map and surface topography of the obtained vortex DOEs by the improved PS-DHM.

This paper is structured as follows. Section 2, explains the azo-polymer synthesis and thin films fabrication procedures. Section 3, describes the interferometric schemes for one-step analog and digital photo-induced relief formation of vortex DOEs based on a vortex phase retarder (VPR) and a SLM, respectively. Section 4, presents the developed PS-DHM system with an embedded liquid crystal variable retarder (LCVR), as well as the calibration of the LCVR. Results of the phase reconstruction and topography characterizing the inscribed DOEs are discussed in Section 4. The conclusions are presented in Section 5.

2. Azopolymer synthesis and thin film fabrication

The photo-sensitive azopolymer was synthesized by the polymerization of the poly-n-epoxypropyl carbazole (PEPC) with azo dye solvent yellow 3 (SY3) chromophore. Solvent Yellow 3 (4'-amino-2,3'-dimethylazobenzene) with dye content 90% is manufactured by Sigma-Aldrich Company, without further purification. Azopolymers were obtained by the reflux method, 0.3 g of PEPC and 0.1 g of SY3, which were dissolved in toluene and refluxed for 8 hours. The reaction of the azo dye attachment to the PEPC polymer matrix was carried out through the epoxy group, which was opened by the primary amine of the azo dye.

After the end of the reaction, the azopolymer solution was cooled and filtered. A polymerization reaction was utilized for chemical bonding of SY3 to PEPC polymer. A chemical structure of PEPC-co-SY3 (3:1) is presented in Fig. 1(a). According to the transmittance spectrum presented

Optics EXPRESS

in Fig. 1(b), for 473 nm wavelength the transmittance is 19% and for 532 nm wavelength the transmittance of the azopolymer is 65%. Fabrication of the azopolymer based thin films was done via spin-coating (using programmable spin-coater "SGS Spincoat G3P-8"). This method offers uniformity as well as high spinning speed resulting in deposition of thin layers in the range of micrometers.

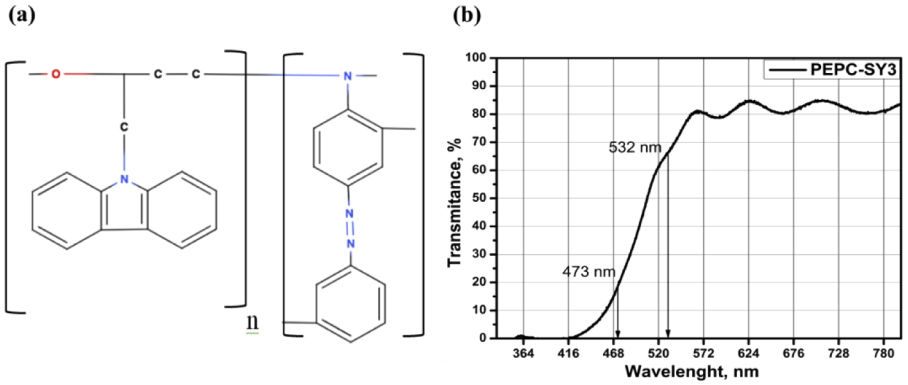

Fig. 1. (a) Chemical structure of the synthesized PEPC-co-SY3 azopolymer; (b) Transmittance spectrum of the synthesized PEPC-co-SY3 azopolymer thin film thickness 1.0 μm.

The coating material PEPC-co-SY3 (10wt.% homogeneous azopolymer) is deposited onto the glass substrate, which is made to rotate and distribute the solution by centrifugal force. The set rotation speed benefits uniform evaporation of the solvent [20]. In the final step, the applied thin film is dried in the oven at 60°C for 6 hours.

The obtained film thickness was determined by using the modified digital MII-4 interference microscope in the reflection mode with magnification of 530^{x} and a depth resolution of 15 nm [16]. The interference patterns of light reflected from the region of the deposed azopolymer and region of the glass substrate were recorded. The developed OpticMeter software was applied for high-accuracy processing of the interferograms [20]. The thickness of the films is equal to 1.0 ± 0.027μm, and is calculated by measuring the corresponding line shifts.

3. Azopolymer surface micro-patterning

3.1. One-step analog polarization holographic recording via VPR

The intensive research in the field of optical materials has shown that light-induced surface deformation in azopolymers is based on the molecular reorientation of the azochromophores perpendicular to the electric field vector of light by a series of trans–cis–trans isomerization cycles. There are still no models fully describing the photo-induced processes in azopolymers, due to the large number of factors that must be considered, such as the reorientation of molecules, change in polymer matrices, the influence of surface forces, mass transfer, changes in optical properties and redistribution of light energy in the formed relief. But, as confirmed by most of researchers, the polarization states of the object and reference beams strongly influence the formation of photo-induced surface gratings.

The first method used for inscribing vortex DOE was the analog PHR with an included VPR as a vortex mask. The VPR (WPV10L from Thorlabs) generates non-diffracting Bessel beams. Specifically, this retarder is a polarization-sensitive plate which transforms the incident Gaussian beam into a "donut hole" Laguerre-Gaussian mode. We have determined that only circular polarization of light preserves the same polarization state after the VPR. So, to ensure the

Optics EXPRESS

orthogonal polarizations, we used right and left circular polarizations (RCP, LCP) of the object and reference beams, respectively.

The sketch of the PHR setup based on a VPR is illustrated in Fig. 2(a). The DOE is produced by interference between a spiral wavefront formed after a laser beam passes through the VPR and a plane wavefront of the reference beam. The VPR generates an OAM with a TC equal to 1. Both interfering beams pass through quarter-wave plates for obtaining a polarized DOE. The angle between interfering beams is approximately $\theta \approx 3.6°$. This angle determines the period of the grating on the X-axis of approximately 7.5μm, calculated by $\Lambda = \lambda/2\sin(\theta/2)$. We underline that the DOEs that are used to create optical vortices are fabricated in a one-step recording process. The resulted diffraction pattern projected on the camera is pictured in Fig. 2(b). The collinearly aligned phase singularities can be observed on the diffraction image.

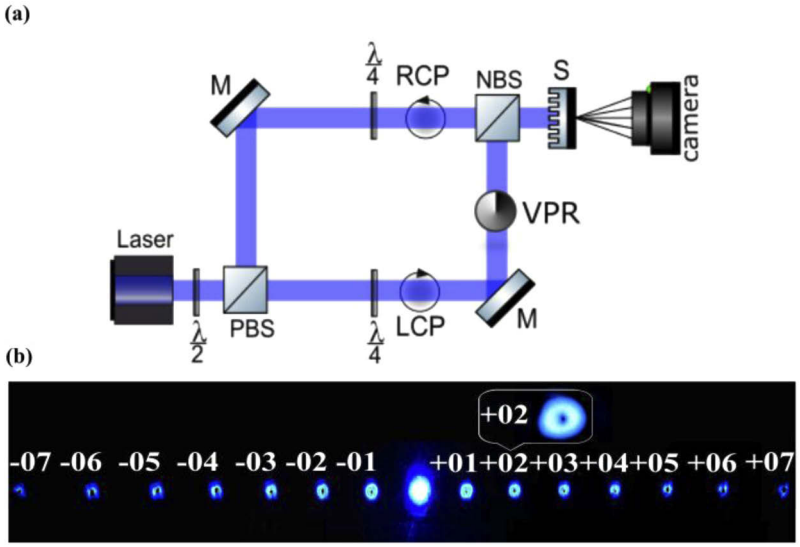

Fig. 2. (a) Analog interferometric arrangement for micro-patterning of vortex DOE via VPR. CW DPSS laser (λ=473 nm, power = 100 mW), M – mirror, PBS – polarized beam splitter, NBS- non-polarized beam splitter, VPR-vortex phase retarder plate, S – sample; λ/4- quarter wave plate, λ/2- half wave plate, camera - 12MPxs camera; (b) image of the phase singularities displayed in the diffraction pattern.

The presence of numerous diffraction maximums (at least 7) points out to the thin grating regime of diffraction. To estimate the performance of the vortex DOE, the diffraction efficiency (DE) evolution was monitored and measured during the recording process, shown in Fig. 3. We note that DE represents an integral characteristic of the diffracted power, which does not take into account its spatial distribution. Nevertheless, DE is one of the main characteristics of the DOE that measures the amount of optical power diffracted into a selected direction (given diffraction order) in comparison with power of the incident beam. The value of DE was measured by the low intensity laser beam with a wavelength $\lambda = 473$ nm. The DE exhibited by the obtained vortex DOE reaches 24% in 12 minutes of exposure. It is measured in the first diffraction order +01 shown in Fig. 2(b).

Although, the applied VPR for PHR provides high diffraction efficiency vortex beams, VPR is a passive optical component that restricts the geometrical variation of azopolymer surface modulation in addition to the limited number of dimensions where the diffraction orders can be spatially distributed. For ensuring dynamic changes in the optical characteristics of the beam shape a SLM was incorporated in the single-beam and dual-beam digital PHR setups.

Optics EXPRESS

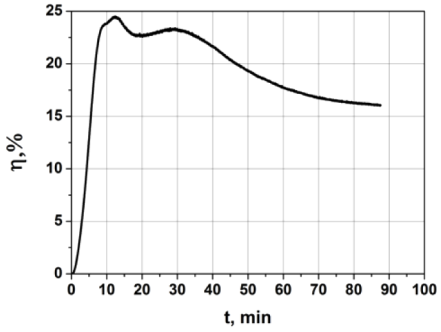

Fig. 3. Kinetics of the first-order diffraction efficiency of the recorded vortex DOE obtained by VPR-based PHR.

3.2. One-step digital polarization holographic recording via SLM

3.2.1. Single-beam polarization holographic recording via SLM

The essence of SLM utilization for PHR is the computer-generated hologram, that involves numerical calculation of the pattern rather than producing it photographically. The phase SLM acts as a sophisticated diffraction grating which transforms the phase of the transmitted light beam into a specific pattern. The phase modulator, in contrast to amplitude one, is more efficient as it completely redirects the incoming light to the outcome image. The dynamic phase range of the SLM (LC2002 HOLOEYE) used in our experiment depends on the wavelength of incident light and is less than 2π for λ=532 nm. Therefore, we displayed a fork-shaped grating (FSG) on the SLM instead of a vortex phase mask. Another issue is that the SLM's pixelated nature affects the generated digital hologram. Particularly, electric field overlapping across the neighboring pixels results in a blurring effect on the sharp edges between pixels. The digital FSG image is incorrectly reconstructed if this limitation is not appropriately solved. Consequently, in our experiment the periodic pattern displayed on the SLM cannot have a period smaller than 20 μm.

The DOE is patterned on the azopolymer thin film by an incident beam that passes through a digital FSG with a TC equal to 2 that was addressed to the SLM display. The PHR setup is pictured in Fig. 4(a). The first polarizer placed before the SLM ensures high extinction ratio of the linear polarization of the input beam. Since SLM changes the polarization of the input beam, to select proper polarization of the output beam the second polarizer is placed after the SLM. When the SLM-generated hologram is illuminated by an incident Gaussian beam, a vortex is created in the output signal. For avoiding the redundant diffraction order caused by SLM screen pixelation, a diaphragm between these lenses was placed.

Low-intensity phase singularities arranged in a single line can be observed in the diffraction image in Fig. 4(b). From the diffraction pattern formed by the vortex DOE recorded on PEPC-co-SY3 thin film we observe that the space distribution of light intensity is "donut-hole" with reduced uniformity of the diffraction maximums. This is proved by DE kinetics presented by black curve in Fig. 6. The maximum DE measured in the first diffraction order +1 is only 0.1% after 180 minutes of exposure.

3.2.2. Dual-beam polarized holographic recording via SLM

The complex vortex DOE was imprinted simultaneously by means of two different recording modes, operating in a parallel regime. The first recording mode functions as the setup described in the section 2.1 with the SLM display located in the object arm of the PHR setup, pictured in Fig. 4(a). The second recording mode functions as a Mach-Zehnder interferometric recording set-up due to adding of the reference arm to the patterning system. The dual-beam PHR setup

Optics EXPRESS

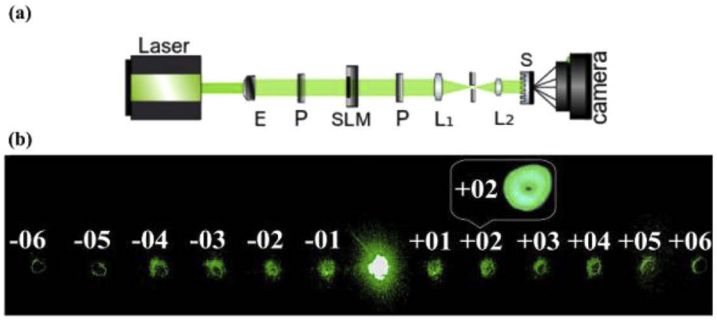

Fig. 4. (a) Digital PHR setup with a single beam. CW DPSS laser (λ=532 nm, power = 2W, TEM_{00}), E-expander, SLM-spatial light modulator LC-2002 with a resolution of 800 × 600 pixels and a pixel pitch of 32 μm, P-polarizer, L1, L2-lenses, S-sample. (b) image of the phase singularities displayed in the diffraction pattern generated by the vortex DOE inscribed by the single-beam PHR via SLM.

is shown in Fig. 5(a). The vortex DOE is formed when the object beam passing through the SLM and possessing -45^0 polarization and the plane Gaussian reference beam possessing $+45^0$ polarization (with regard to the plane of interfering beams) interfere. In this way, the angle between polarization states of the interfering beams is 90^0.

As shown in our previous investigations [16], cross-polarized states of light beams controlled by half-wave plates facilitate the maximum surface relief modulation. The half-wave plate placed immediately after the laser controls the polarization direction of the incident beam with regard to the beam splitter. The polarized beam-splitter provides 30:70 intensity ratio with a minimal dependence on the polarization state of the incident light. For covering the entire SLM matrix, the incident beams were expanded. To scale the hologram transmitted through SLM in correspondence to the recording spot on the film, two lenses with different focal lengths were used.

The photo-induced vortex DOE generates multi-channel vortex beams, as shown in Fig. 5(b). The phase singularities arranged in multiple lines can be observed in the diffraction pattern displayed on the camera. The diffraction image has a 2D space distribution. The distribution of diffraction maximums along X-axis coincides with the space distribution maximums obtained by single-beam recording via SLM described in Fig. 4 (b). The diffraction maximums along Y-axis are significantly bigger and brighter, and the distance between them corresponds to the 5.0 μm grating period.

We can suppose that the recorded DOE consists of two surface gratings in X and Y directions of the sample plane. The grating period on the X-axis resulting from the first recording mode is 20.0 μm and is tuned by the frequency of the hologram fringes displayed on the SLM. The grating period on the Y-axis resulting from the second recording mode is 5.0 μm, and is determined by the angle $\theta \approx 6^0$ between reference and the object waves beams of the optical setup. The black curve in Fig. 6 shows the DE evolution measured online in the +01-diffraction order obtained by dual-beam recording setup and coincides with the +01-diffraction order obtained via single-beam recording setup. The DE value in +01 diffraction order is about 0.1%. The red curve describes the DE evolution in the +13-diffraction order. The DE value reaches 3.5% in 180 minutes of exposure.

It is important to note that the DEs measured from the obtained DOEs represent a relative value because it comprises the entire "donut-hole" including the isolated intensity zero present in the phase singularity. Thus, when excluding the regions with zero intensity, the real efficiency might be higher.

Optics EXPRESS

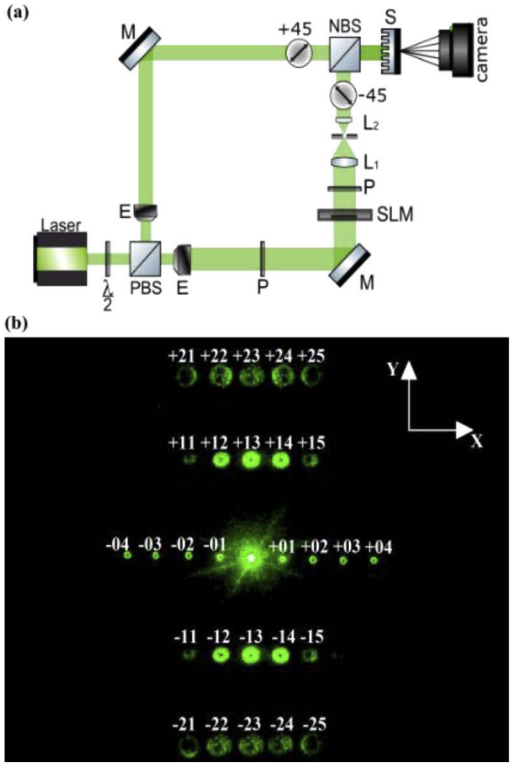

Fig. 5. (a) Digital dual-beam PHR setup for micro-patterning complex vortex DOE that generate spatial multiplexed phase singularities. CW DPSS laser (λ=532 nm, power = 2W, TEM_{00}), M – mirror, PBS – polarized beam splitter, NBS- non-polarized beam splitter, E-expander, SLM-spatial light modulator LC-2002 with a resolution of 800 × 600 pixels and a pixel pitch of 32 μm, S – sample; λ/2- half wave plate, P-polarizer, L1, L2-lenses, (b) the spatial multiplexed diffraction pattern obtained via dual-beam digital PHR.

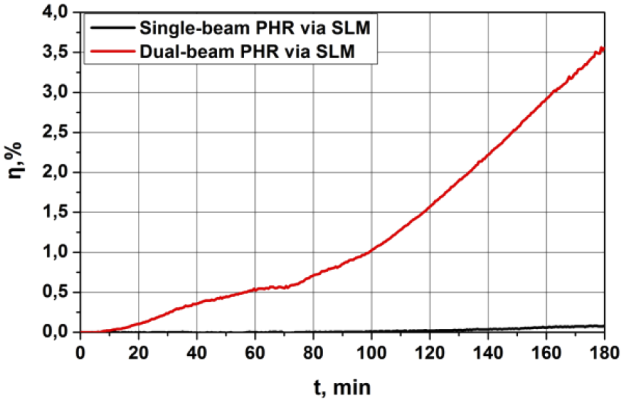

Fig. 6. Kinetics of the diffraction efficiency of the recorded vortex DOEs obtained by PHR via SLM.

Optics EXPRESS

4. PS-DHM phase imaging system of vortex DOEs

PS-DHM was applied to examine the DOEs recorded on the azopolymer thin films. The main advantage of PS-DHM is the high accuracy of the hologram acquisition. It is mainly due to the full-coverage of the camera sensor's active area. In addition, PS-DHM is performed without frequency filtering usually required for separating the conjugate and the zero-order images in the off-axis configuration. Still, one of the PS-DHM drawbacks is the presence of mechanical movement performed by phase-shifting devices.

Our PS-DHM system was upgraded with the LCVR to perform phase shifts in the reference beam. The merit of the developed PS-DHM is that LCVR executes optical phase shifting, by driving voltages, with higher accuracy if compared to mechanical displacement, produced via a piezoelectric transducer. In particular, this is because LCVR is mounted in-line, vibration free, and functions more stable by producing high retardance uniformity [21]. Furthermore, automatic control of the LCVR adopted in LabVIEW software permits the holograms frame registration within 30 milliseconds. Thus, fast hologram acquisition minimizes the periodic background noise and temperature variation typically influencing the image quality.

4.1. LCVR calibration

The LCVR must be preliminary calibrated to perform a precise phase control. The aim of the calibration is to determine the dependence of the phase retardance on the applied voltage without changing the polarization of the input beam. For this purpose, an off-axis digital holographic registration scheme was used with subsequent restoration of the phase pattern by the Fast Fourier Transform method. To control the polarization for the set of phase shifts, it is necessary to correctly adjust the anisotropy axes of the LCVR. Pure phase modulation was achieved by setting the optical fast(slow)axis of the LCVR at an angle of 0°(90°) with respect to the polarization of the incident beam. The fine adjustment of the LCVR's axes was performed by Thorlabs' PAX1000VIS Polarimeter (Azimuth and Ellipticity Accuracy of ±0.25°)

The predominantly phase modulation was verified with an additional polarizer placed after the LCVR and intensity analysis on a CMOS camera. When the voltage across the phase plate was changed from 0 to 10 V, the intensity observed on the camera was invariant, which indicates that the phase is modified while the polarization state remains constant.

Figure 7 shows the reconstructed phase retardance of the LCVR, depending on the applied voltage (with a step of 0.1 V). A more accurate analysis of the phase retardance was performed in the quasi-linear section $\Delta\varphi(V)$ 1.5-3.5 V with a step of 0.05 V and the dependence for three series of measurements, with a voltage change of 1.5-3.5 V and vice versa 3.5-1.5 V. To produce particular phase shifts (PS) equal to $\varphi_1=0$, $\varphi_2=\pi/2$, $\varphi_3=\pi$, $\varphi_4=3\pi/2$ a linear approximation of the LCVR phase shift in the region 2-3.2 V of the applied voltages was carried out. The initial applied voltage is 2.02 V where the phase shift is considered null. The phase step is equal to $\pi/2$. After calculations, it was determined that the four phase changes pointed above correspond to the voltages $V_1 = 2.02$ V, $V_2 = 2.39$ V, $V_3 = 2.76$ V, $V_4 = 3.14$ V, respectively.

4.2. PS-DHM optical configuration

The outline of the PS-DHM without moving components is depicted in Fig. 8. In the experiment, the single-mode laser beam is divided by a non-polarized beam-splitter into the undisturbed reference wave-R_w and the scattering from the vortex DOE- O_w. Laser beam diameters are expanded by a microscope objective and lens L_2. The collimated object beam passes through a half-wave plate to adjust the polarization states of the object and reference beams. The second lens focuses light on the sample. The CMOS camera acquires digital holograms via identical microscopic systems in both paths. The microscope magnification was evaluated by preliminary calibration using a 1 mm stage micrometer with 10 μm divisions. It was determined that each

Optics EXPRESS

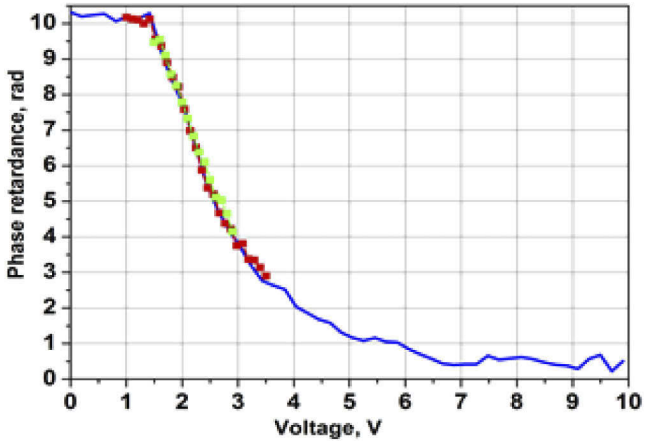

Fig. 7. Reconstructed phase retardance for the laser wavelength 532 nm of the LCVR (LCVR-100"Medowlark optics" with a modulation resolution of 1mV and contrast value of the polarization state -150:1) depending on the applied voltage, measured with a step of 0.1 V (blue) and analysis of the phase retardance in the quasi-linear range 1.5-3.5 V with a step of 0.05 V for three series of measurements (blue, red and green).

CMOS pixel acquires 160×160nm of the sample area. The phase of the reference beam is shifted sequentially by the LCVR. Nematic liquid crystals producing the phase retardations exhibit optical birefringence properties. Therefore, half-wave plates are introduced in each arm for maintaining similar polarization of both beams and to achieve high-contrast interference patterns. The object wave is superposed with the reference wave after a non-polarized beam splitter, and then the combined beams form the in-line hologram on the CMOS camera.

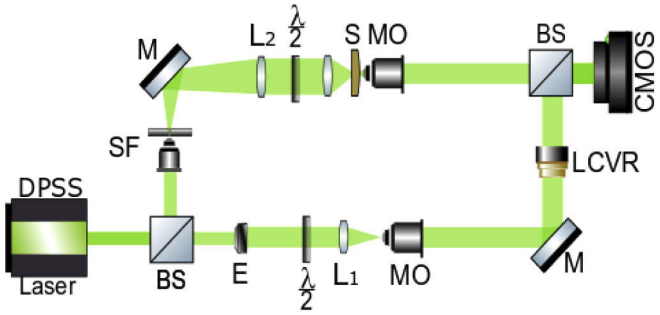

Fig. 8. DHM setup:CW DPSS laser (λ=532nm, 100 mW, TEM_{00}), BS-non-polarized beam splitter, λ/2- half-wave plates, M-mirror, MO-microscope objective (20^{x}, NA=0.40), S-sample, L1, L2-lenses, CMOS- digital camera "DMK33UX264", resolution 2,448×2,048 (5 MPxs), LCVR- "Meadowlark optics" liquid crystal variable retarder LCVR-100, SF-spatial filter, E-beam expander.

The digital hologram recorded by the CMOS camera is a result of the interference of the object beam O_w=$A_O$exp($i\Phi_O$) and reference beam R_w=$A_R$exp$i$(Φ_R+φ_N), whose intensity is given by

$$I_N = |O_W + R_W|^2, \tag{1}$$

where A_O, A_R and Φ_O, Φ_R are the amplitudes and the phases of the object and reference waves, respectively, and φ_N represents the phase changes in the reference arm created by the LCVR, where N=1, 2, 3, 4.

Optics EXPRESS

The phase can be quantitatively reconstructed from the four recorded interferograms using the procedure first proposed by I. Yamaguchi in [22]:

$$\Delta\Phi = \tan^{-1}\left[\frac{I_1 - I_3}{I_2 - I_4}\right], \tag{2}$$

where I_1, I_2, I_3, I_4 are the intensities of the four-step PS interferograms with the corresponding phase changes mentioned above.

For reconstructing the phase map of the DOEs four object holograms are captured within the DOE recorded in the azopolymer film. Another four reference holograms are recorded on the unprocessed area of the film for minimizing the background effect and the modulation fluctuations. Finally, the phase map of the DOE is calculated by:

$$\Delta\Phi(x, y) = \Delta\Phi_O(x, y) - \Delta\Phi_R(x, y), \tag{3}$$

where $\Delta\Phi_O(x,y)$, $\Delta\Phi_R(x,y)$ are reconstructed phase maps from the object and reference holograms, respectively. The reconstruction algorithm executes the numerical compensation of the PS in case of misaligned shift produced by the LCVR. This step is important when the environmental disturbances influence the laboratory conditions (temperature changes, excessive building vibrations, etc.). A small phase shift is added during the phase reconstruction stage until the object phase is successfully revealed. After the PS compensation, phase unwrapping is performed by PUMA unwrapping algorithm based on energy minimization, first described in [23].

4.3. PS-DHM results and discussions

Knowledge of deposited azopolymer thin films behavior under the influence of light interference is valuable for determining the quality of the formed patterns, as well as for measuring surface photo-induced deformations in different directions of the vortex DOEs. The topography (Δh) of the vortex DOEs is calculated numerically from the unwrapped phase by

$$\Delta h(x, y) = \frac{\Delta\Phi(x, y)}{2\pi(n - 1)}\lambda, \tag{4}$$

where λ=532nm is the wavelength and n is the refractive index of the azopolymer films.

Generally, two kinds of phenomena govern the formation of diffraction gratings in azopolymers: 1. Volume birefringence due to photo-induced modulation of the refractive index; 2. Surface relief modulation caused by the mass movement, triggered by structural photo-induced modifications in the bulk of the azopolymer [24]. Even though obtained DOEs can be considered as birefringence gratings, the contribution of the refractive index to the overall DE of azopolymer thin films is relatively small [25]. On this basis, it is important to mention that only the surface relief modulation is considered while the refractive index changes in azopolymers are not taken into account in our calculations. The reconstructed phase map from the PS-DHM holograms includes both bulk and surface phase modulation of the azopolymer films.

The PS-DHM measurement results of the vortex DOE obtained using the analog PHR setup based on a VPR are illustrated in Fig. 9(a) and Fig. 9(b). It has a form of a FSG with one groove bifurcation and TC equal to 1, respectively. The mean value of height for this DOE is equal to 250 nm as shown in the cross-section depicted in Fig. 9(c). The grating period is approximately 7.5 μm, which corresponds to the experimental recording conditions. The highlighted black line on the 3D topography map denotes the line along which the cross-section was extracted.

Figure 10 shows the microscope result images of the vortex DOE patterned using the digital single-beam PHR setup based on a SLM. In Fig. 10(a) and Fig. 10(b) is shown the topography map of the FSG with the TC equal to 2. According to the cross-section depicted in Fig. 9(c), the mean value of surface relief height is 157 nm and the period of the grating is 20 μm.

Optics EXPRESS

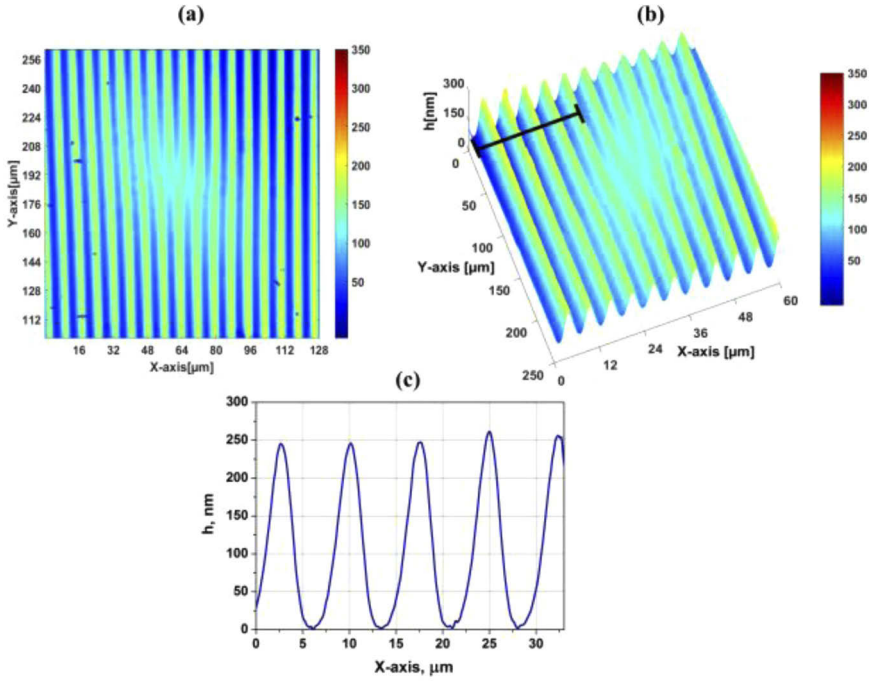

Fig. 9. (a) 2D phase image, (b) 3D topography map and (c) X-axis cross-section of vortex DOE recorded via analog PHR setup.

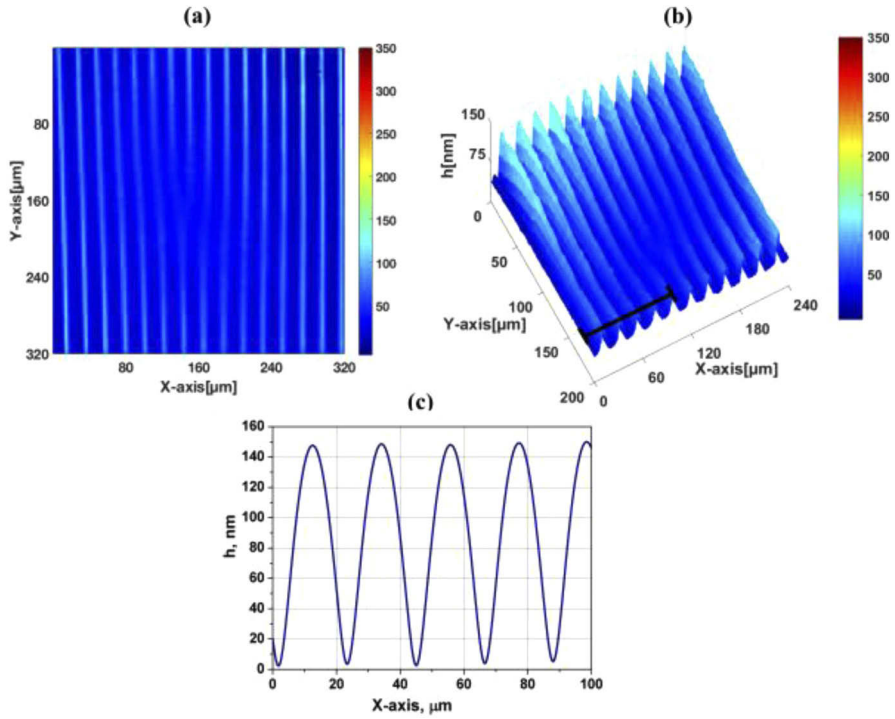

Fig. 10. (a) 2D phase image, (b) 3D topography map (c) X-axis cross-section of the vortex DOE recorded via digital single-beam PHR setup.

Optics EXPRESS

The reconstructed full-field surface of the complex vortex DOE inscribed via dual-beam SLM-based setup is pictured in Fig. 11. The central part of complex vortex DOE is seen more clearly if compared to the DOE obtained via single-beam PHR. Two-fold symmetrically spaced fringes along the X- and Y-directions of the relief map result from the one-step PHR of two orthogonal modes. The cross-section built across the Y-axis, shown in Fig. 11(c), reveals the relief slopes with a height of 300 nm and a frequency of 5.0 μm, created by the intersection of the SLM modulated beam and the object wave with polarization states of $+45^0$:-45^0, respectively. Surface profile extracted across the X-axis presented in Fig. 11(d) denotes the azopolymer films structuring by the digital fork-shaped hologram addressed to the SLM. A grating with two peaks was observed on the X-axis: the major peak with depth about 300 nm, and additional minor peaks with a height of 50 nm. The period of the patterned fringes is 20.0 μm and corresponds to the fork grating displayed on the SLM. The origin of minor peaks could be the result of the refractive index modulation in the azopolymer films. We think that the variation of the surface relief height and diffraction efficiency of the DOEs obtained by analog and digital PHR is explained by different period of the recorded gratings that also influences on these parameters. In addition, the absorption of the azopolymer at 473nm is higher than at 532nm wavelength of the recording beam. Slightly increased roughness of the complex DOE may be the outcome of increased sensitivity to the pixilated nature of SLM, and external vibrations of the patterning setup. Additional investigations of the surface deformation have to be performed for exact estimation of the surface and volume contributions in the phase image of the grating.

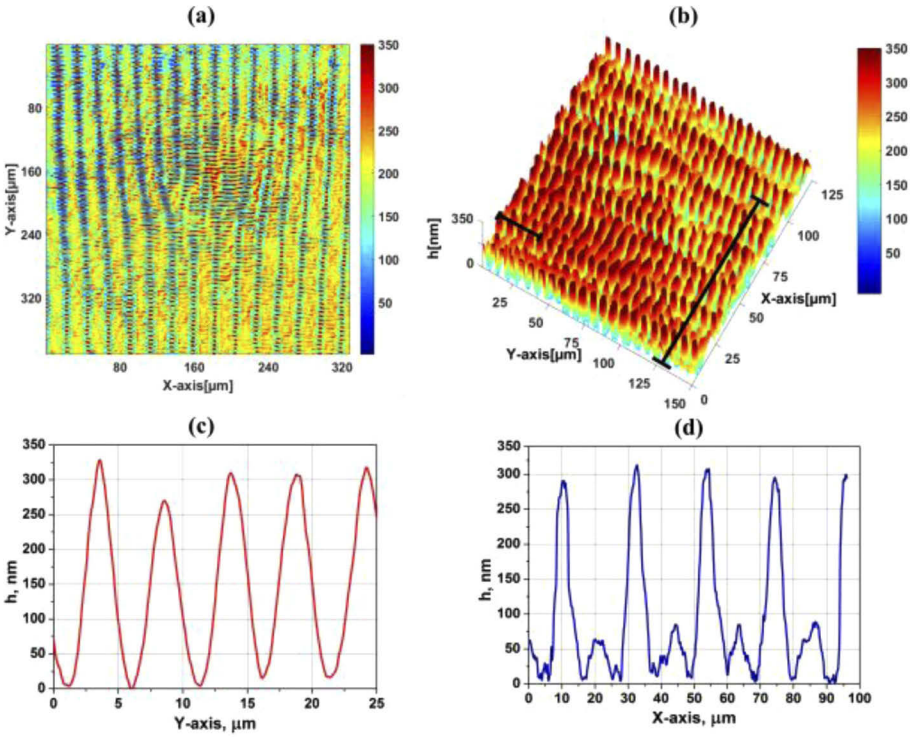

Fig. 11. (a) 2D phase image, (b) 3D topography map (c) Y-axis cross-section (d) X-axis cross-section of the complex vortex DOE patterned by digital dual-beam PHR.

Optics EXPRESS

5. Conclusions

Our paper highlights vortex DOEs as final product of digital and analog polarization holographic recording on the new azopolymer thin films. Spiral wavefront generated by analog PHR via VPR produces DOEs that create vortex beams with high diffraction efficiency, however the variability of the spatial distribution of the diffraction pattern is limited. In contrast, the digital generation of the spiral wavefront by SLM introduced in the PHR system is a more flexible source that permits to record DOEs that generate 2D and 3D spatial distribution of the diffraction patterns. The specific advantage of our results is the combination of PHR with new polarization-sensitive azopolymer, that permits to obtain DOEs with deep surface relief of about 40% with respect to the total thin film thickness.

We have presented the designing process of three types of DOEs on carbazole-based azopolymers capable of generating single-channel and spatial multiplexed phase singularities. The implemented analog and digital PHR in different optical setups have proven to be an efficient one-step method for patterning vortex DOEs that generate phase singularities. Although it seems that both approaches permit to fabricate DOEs that produce similar fields, the variation of the vortex beams parameters must be considered. The highest diffraction efficiency is exhibited by the DOE patterned via an analog VPR, while the DOE obtained by the digital single-beam interferometric setup with an embedded SLM produces vortices with the lowest diffraction efficiency and smallest surface modulation of azopolymer thin film. The complex DOE recorded by the digital dual-beam interferometric setup generates multiple channels with phase singularities and has the maximum surface modulation.

The advanced PS-DHM with the incorporated LCVR was developed for non-contact, all-optical investigation of the phase and surface relief transformations. We have proven that the proposed PS-DHM configuration can be successfully used as a metrological tool for 3D quantitative measurements of complex structures including transparent surface relief deformations on a nanometer scale.

We anticipate that in future, extended research on the input of surface relief and refractive index changes into the phase modulation of the azopolymer thin films would further facilitate complete understanding of the behavior as well as the photonic applications of these materials.

Funding. Teknologiateollisuuden 100-Vuotisjuhlasäätiö; Jane and Aatos Erkko Foundation and Finland Centennial Foundation funded "Computational Imaging without Lens" (3122800139); The World Federation of Scientists (National Scholarship Programme); Bilateral project Moldova-Belarus project (25/31.07/18, Bilateral project Moldova-Belarus project); Content NARD of Republic of Moldova (20.70086.16/COV (01.07.2020-30.06.2021), BIOHOLO project).

Disclosures. The authors declare no conflicts of interest.

References

1. F. Nye and M. V. Berry, "Dislocations in Wave Trains," Proceedings of Royal Society A on Mathematical, Physical and Engineering Sciences **336**(1605), 165–190 (1974).
2. Y. Liang, Y. Cai, Z. Wang, M. Lei, Z. Cao, Y. Wang, M. Li, S. Yan, P. R. Bianco, and B. Yao, "Aberration correction in holographic optical tweezers using a high-order optical vortex," Appl. Opt. **57**(13), 3618–3623 (2018).
3. I. Augustyniak, A. Popiołek-Masajada, J. Masajada, and S. Drobczyński, "New scanning technique for the optical vortex microscope," Appl. Opt. **51**(10), C117–C124 (2012).
4. A. Jesacher, A. Schwaighofer, S. Fürhapter, C. Maurer, S. Bernet, and M. Ritsch-Marte, "Wavefront correction of spatial light modulators using an optical vortex image," Opt. Express **15**(9), 5801–5808 (2007).
5. F. Cardano, E. Karimi, S. Slussarenko, L. Marrucci, C. de Lisio, and E. Santamato, "Polarization pattern of vector vortex beams generated by q-plates with different topological charges," Appl. Opt. **51**(10), C1–C6 (2012).
6. X.-C. Yuan, J. Lin, J. Bu, and R. E. Burge, "Achromatic design for the generation of optical vortices based on radial spiral phase plates," Opt. Express **16**(18), 13599–13605 (2008).
7. M. Szatkowski, J. Masajada, I. Augustyniak, and K. Nowacka, "Generation of composite vortex beams by independent Spatial Light Modulator pixel addressing," Opt. Commun. **463**, 125341 (2020).
8. V. Arrizón, U. Ruiz, D. Sánchez-de-la-Llave, G. Mellado-Villaseñor, and A. S. Ostrovsky, "Optimum generation of annular vortices using phase diffractive optical elements," Opt. Lett. **40**(7), 1173–1176 (2015).
9. L. Stoyanov, S. Topuzoski, I. Stefanov, L. Janicijevic, and A. Dreischuha, "Far field diffraction of an optical vortex beam by a fork-shaped grating," Opt. Commun. **350**, 301–308 (2015).

Optics EXPRESS

10. O. Barlev and M. A. Golub, "Multifunctional binary diffractive optical elements for structured light projectors," Opt. Express **26**(16), 21092–21107 (2018).
11. Y. Shen, X. Wang, Z. Xie, C. Min, X. Fu, Q. Liu, M. Gong, and X. Yuan, "Optical vortices 30 years on: OAM manipulation from topological charge to multiple singularities," Light: Sci. Appl. **8**(1), 90 (2019).
12. S. Li and Z. Wang, "Generation of optical vortex based on computer-generated holographic gratings by photolithography," Appl. Phys. Lett. **103**(14), 141110 (2013).
13. P. Vayalamkuzhi, K. Keskinbora, C. T. Samlan, M. Hirscher, J. P. Spatz, and N. K. Viswanathan, "Direct patterning of vortex generators on a fiber tip using a focused ion beam," Opt. Lett. **41**(10), 2133–2136 (2016).
14. R. Fernandez, S. Gallego, A. Marques, C. Neipp, E. M. Calzado, J. Frances, M. Morales-Vidal, and A. Belendez, "Complex Diffractive Optical Elements Stored in Photopolymers," Polymers **11**(12), 1920 (2019).
15. V. M. Kryshenika, Y. M. Azhniuka, and V. S. Kovtunenko, "All-optical patterning in azobenzene polymers and amorphous chalcogenides," J. Non-Cryst. Solids **512**, 112–131 (2019).
16. A. Meshalkin, S. Robu, E. Achimova, A. Prisacar, D. Shepel, V. Abashkin, and G. Triduh, "Direct photoinduced surface relief formation in carbazole-based azopolymer using polarization holographic recording," J Optoelectron. Adv. M. **18**(9-10)), 763–768 (2016).
17. N. K. Viswanathan, S. Balasubramanian, L. Li, S. K. Tripathy, and J. Kumar, "A Detailed Investigation of the Polarization-Dependent Surface-Relief-Grating Formation Process on Azo Polymer Films," J. Appl. Phys. **38**(10), 5928–5937 (1999).
18. J. A. Picazo-Bueno, M. Trusiak, and V. Micó, "Single-shot slightly off-axis digital holographic microscopy with add-on module based on beamsplitter cube," Opt. Express **27**(4), 5655–5669 (2019).
19. V. Cazac, A. Meshalkin, E. Achimova, V. Abashkin, V. Katkovnik, I. Shevkunov, D. Claus, and G. Pedrini, "Surface relief and refractive index gratings patterned in chalcogenide glasses and studied by off-axis digital holography," Appl. Opt. **57**(3), 507–513 (2018).
20. A. Meshalkin, V. Abashkin, A. Prisacar, G. Triduh, I. Andries, L. Bets, and E. Achimova, "High precision interferometric thickness analysis of submicrometers spin-coated polyepoxupropylcarbazole films," Sensor Electronics and Microsystem Technologies **3**, 62–69 (2012).
21. P. Bouchal, R. Celechovsk, and Z. Bouchal, "Polarization sensitive phase-shifting Mirau interferometry using a liquid crystal variable retarder," Opt. Lett. **40**(19), 4567–4570 (2015).
22. I. Yamaguchi and T. Zhang, "Phase-shifting digital holography," Opt. Lett. **22**(16), 1268–1270 (1997).
23. I. Shevkunov, "A new phase unwrapping method," J. Phys.: Conf. Ser. **737**, 012065 (2016).
24. S. Moujdi, Y. Bougdid, A. Rahmouni, T. Mahfoud, D. Nesterenko, M. Halim, and Z. Sekkat, "Azo-polymers for holographic recording: photo-assisted holography and surface relief gratings," Proc. SPIE **10944**, 1094403 (2019).
25. A. Priimagi and A. Shevchenko, "Azopolymer-based micro- and nanopatterning for photonic applications," J.Polym. Sci. B, Polym. Phys **52**(3), 163–182 (2014).